Molecular Cancer Research

Senescent Carcinoma-Associated Fibroblasts Upregulate IL8 to Enhance Prometastatic Phenotypes

Tao Wang[1,2,3], Faiyaz Notta[4], Roya Navab[1], Joella Joseph[1,3], Emin Ibrahimov[1,4], Jing Xu[1], Chang-Qi Zhu[1], Ayelet Borgida[5], Steven Gallinger[6,7], and Ming-Sound Tsao[1,2,3]

Abstract

Carcinoma-associated fibroblasts (CAF) represent a significant component of pancreatic cancer stroma and are biologically implicated in tumor progression. However, evidence of both cancer-promoting and -restraining properties amongst CAFs suggests the possibility of multiple phenotypic subtypes. Here, it is demonstrated that senescent CAFs promote pancreatic cancer invasion and metastasis compared with nonsenescent control CAFs using *in vitro* Transwell invasion models and *in vivo* xenograft mouse models. Screening by gene expression microarray and cytokine ELISA assays revealed IL8 to be upregulated in senescent CAFs. Experimental modulation through IL8 overexpression or receptor inhibition implicates the IL8 pathway as a mediator of the proinvasive effects of senescent CAFs. In a cohort of human pancreatic cancer cases, more abundant stromal senescence as indicated by p16 immunohistochemistry correlated with decreased survival in patients with early-stage disease. These data support senescent fibroblasts as a pathologically and clinically relevant feature of pancreatic cancer. The inhibition of senescent stroma–cancer signaling pathways has the potential to restrain pancreatic cancer progression.

Implications: Findings show that senescent cancer-associated fibroblasts secret excess IL8 to promote pancreatic cancer invasion and metastasis; thus, senescent CAFs represent a phenotypic subtype, challenging conventional assumptions that CAFs are a homogeneous population. *Mol Cancer Res; 15(1); 3–14. ©2016 AACR.*

Introduction

Pancreatic ductal adenocarcinoma (PDAC), the predominant form of pancreatic cancer, is a highly lethal malignancy with 5-year survival rates of less than 7% (1). PDAC is well-known to have intense stromal fibrosis (desmoplasia), which often forms the majority of the physical tumor volume (2, 3). The desmoplasia results from the activation of quiescent pancreatic stellate cells into cancer-associated fibroblasts (CAF) in response to transforming growth factor beta (TGFβ) and platelet-derived growth factor (PDGF) ligands derived from carcinoma cells and inflammatory cells (4–6). The activated CAFs assume a myofibroblastic phenotype and secrete growth factors and cytokines (4–6). Our understanding of the interaction between PDAC and CAFs has evolved in recent years. CAFs were initially shown to promote cancer growth, invasion, angiogenesis, and metastasis in a number of solid cancers (5, 7–9). For many years, the concept that CAFs were cancer-promoting cells has been the prevailing view. However, in recent genetically engineered mouse models of pancreatic cancer, depletion of smooth muscle actin (α-SMA)-expressing myofibroblasts or inhibition of the stromal mediated hedgehog pathway accelerated disease and led to worse outcomes (10–12). These results challenge the traditional views of CAFs and raise the possibility that they are actually a phenotypically heterogeneous population.

The phenotypic changes that occur as a result of cellular stress and aging provide a potential source of fibroblast heterogeneity. When proliferating cells are subjected to stress from DNA damage, telomere shortening, chromosomal alteration, or oxidative stress, they can enter permanent growth arrest or senescence (13, 14). Similar to CAFs, senescent fibroblasts derived from normal tissue have been shown to promote progression of a variety of cancers, including prostate, melanoma, head and neck, and breast (15–18). Senescent fibroblasts possess a senescence-associated secretory phenotype (SASP), which involves selective overexpression of many secreted factors, most commonly Interleukin 6 (IL6) and Interleukin 8 (IL8), CXC motif ligand 1 (CXCL1), as well as various matrix metalloproteinases and serine proteases (13, 19, 20). It is unknown whether CAFs possess senescent features *in vivo*. Moreover, it is unknown whether the senescent CAF phenotype can influence the pathogenesis of PDAC.

The modulation of the cancer–stromal interaction is an area of intense scientific and clinical investigation. Identifying specific populations of stromal cells and their interaction pathways may elucidate novel targets for stromal-directed therapies. To account for the apparently divergent roles of CAFs, as well as the overlapping properties of senescent fibroblasts and CAFs, we will demonstrate that senescent CAFs are a pathologically relevant fibroblast phenotype in pancreatic cancer.

[1]Princess Margaret Cancer Centre, University Health Network, Toronto, Canada. [2]Department of Pathology, University Health Network, Toronto, Canada. [3]Department of Laboratory Medicine and Pathobiology, University of Toronto, Toronto, Canada. [4]Ontario Institute for Cancer Research, Toronto, Canada. [5]Zane Cohen Centre for Digestive Diseases, Mount Sinai Hospital, Toronto, Canada. [6]Department of General Surgery, University Health Network, Toronto, Canada. [7]Department of Surgery, University of Toronto, Toronto, Canada.

Note: Supplementary data for this article are available at Molecular Cancer Research Online (http://mcr.aacrjournals.org/).

Corresponding Author: Ming-Sound Tsao, Toronto Medical Discovery Tower 14-401, 101 College Street, Toronto, ON, Canada M5G 1L7. Phone: 416-634-8721; Fax: 416-340-5517; E-mail: ming.tsao@uhn.ca

doi: 10.1158/1541-7786.MCR-16-0192

Materials and Methods

Cell lines, tissue, and mouse strains

This study was approved by the Research Ethics Board of the University Health Network (13-6377). Fresh samples of surgically resected PDAC were minced, digested with collagenase (Worthington), and plated to derive primary pancreatic CAFs. Pancreatic cancer cell lines MiaPaca2 and Panc-1 were obtained from the ATCC and L3.6pl from the MD Anderson Characterized Cell Line Core Facility (Houston, TX), with identities confirmed by short tandem repeat testing. $CAF094^{YFP\text{-}hTERT}$ (CAF094) fibroblasts were derived from a non–small cell lung cancer in our laboratory and immortalized using lentiviral transduction of hTERT (8).

All cell lines were cultured in DMEM (MiaPaca2, Panc1, CAF094) or DMEM/HamF12 (L3.6pl, Pancreatic CAFs) with 10% FBS at 37°C in 5% CO_2. Formalin-fixed, paraffin-embedded human PDAC tissue was obtained from adult patients diagnosed with pancreatic ductal adenocarcinoma between 2008 and 2015 who consented to have tissue allocated for research. Mouse experiments were performed with 6-week-old male mice of the NOD/SCID gamma (NSG) strain (The Jackson Laboratory) and were approved by the UHN Animal Resource Centre.

Cell growth assay

The xCelligence RTCA system (ACEA Biosciences) was used for growth assays, with 4,000 cells plated per well in complete media. Cell index was normalized at the nadir time point and hourly measurements were taken for 100 hours.

Induction of senescence

To induce replicative senescence, confluent CAFs were passaged until morphologic signs of senescence emerged along with cessation of growth. For induction of senescence by H_2O_2, cells were exposed to 550 μmol/L peroxide in complete culture media for 2 hours. Cells were passaged the next day and left for at least 1 week prior to use. β-Galactosidase assay was performed to confirm senescence (14). Cultures with more than two thirds of cells showing moderate to strong staining would be considered senescent. Because of the finite replication potential of primary culture pancreatic CAFs, we used parental CAF lines between passages 4 and 7 with less than 20% senescent cells as nonsenescent controls.

Immunofluorescence and immunohistochemistry

Immunofluorescence was performed on cultured cells using antibodies at various concentrations (Supplementary Table S1, Supplementary Methods). Immunohistochemistry (IHC) was performed using a Ventana Benchmark XT using antibodies at various concentrations (Supplementary Methods). For p16 (*CDKN2A*) and IL8 IHC, scanned slides were annotated by a pathologist (T. Wang) and analyzed by the "Positive Pixel Count v9" algorithm with Aperio ImageScope (Leica Biosystems). For analysis of stromal signal, areas of carcinoma, lymphoid follicles, large nerves, and vasculature were excluded by pathologist annotation. For analysis of total tumor, both stromal and carcinoma signals were included. For p16, pixels with moderate to strong intensity were considered positive. For IL8, pixels with strong staining (as determined by the software algorithm) were assigned a weight of 3, moderate a weight of 2, and weak a weight of 1, with final scores normalized to a maximum of 1.0.

RNA *in situ* hybridization

Paraffin-embedded PDAC tissue underwent RNA *in situ* hybridization (ISH) as per manufacturer protocols using the RNAscope system (Advanced Cell Diagnostics) with probes for IL8 (ACD#310381) and controls.

Transduction and Western blot

MiaPaca2 was transduced with pLKO.luciferase.YFP using a lentiviral system as previously described (21, 22). The resultant MiaPaca2-YFP cells were enriched with a Becton Dickinson Biosciences FACSAria cell sorter (Supplementary Fig. S1). pLD.IL8-3xFlag was created by cloning IL8 ORF (Open Biosystems; clone ID 100008187) into the pLD.puro.DEST.3xFlag vector using the Gateway System (Thermo Fisher). $CAF094^{YFP\text{-}hTERT}$ immortalized lung cancer fibroblasts were transduced with pLD.IL8-3xFlag or pLD empty vector, followed by selection with 1 μg/mL of puromycin (8). Overexpression of Flag-tagged IL8 was confirmed by Western blotting with MAB208 IL8 antibody (R&D Systems) and #2368 anti-FLAG antibody (Cell Signalling Technology) using 24-hour conditioned media of transduced CAF094 cells with 0.5% serum (Supplementary Methods).

Transwell invasion assays

For invasion assays, 24-well format, 8.0-μm pore (transparent or Fluoroblok), membrane-covered inserts (Corning Inc.) were coated with 60 μL of 233 μg/mL Matrigel at 37°C for 3 hours. Cancer cells (50,000) were added to the insert and CAFs (60,000 for primary lines 4 or 5; 100,000 for $CAF094^{EV}$ or $CAF094^{IL8\text{-}3xFlag}$) were added to the bottom well in 0.2% (for primary CAFs) or 0.5% (for CAF094) serum media and incubated for 24 hours. For Fluoroblok membranes, invaded cells were counted on an Axio Observer fluorescent inverted microscope (Zeiss) over 5 mm^2. For transparent membranes, cells were fixed with 0.5% glutaraldehyde and stained with 0.2% crystal violet (EMD Chemicals) for 4 hours. Noninvaded cells were wiped away with a cotton tip and the membranes were mounted on slides. Invaded cells were counted over 2.5 mm^2 by brightfield microscopy.

IL8 inhibitor assays

Reparixin (ApexBio) or SB225002 (Cayman Chemical) were added to 96-well Transwell Fluoroblok system (Corning) at various concentrations. Top wells contained 10,000 MiaPaca2-YFP cells and the bottom contained blank controls or 20,000 CAFs. Invaded fluorescent cells were counted on the Zeiss Axio Observer over 4 mm^2.

For reparixin and SB225002, toxicity assays were performed by 24 hours of incubation at varying concentrations with 40,000 MiaPaca2-YFP or 20,000 CAF cells cultured in 24-well plates. Conditioned media and trypsinized cells were collected and centrifuged at 1,200 × *g* for 5 minutes. Cells were then counted by hemocytometer with a 1:1 mixture of trypan blue. Cells positive for trypan blue were considered to be dead.

Indirect coculture growth assays

CAFs (20,000 of CAF1 or CAF2) were seeded onto 24-well format, 0.4-μm pore Transwell inserts, and cancer cells (5,000 Panc1 or L3.6) were seeded on the companion plate. Cancer cells were counted every 2 days.

RNA isolation, cDNA synthesis, and quantitative real-time PCR

RNA was isolated from a 10-cm dish of cultured cells using TRIzol (Life Technologies). The specimen was digested with DNAse (Life Technologies/Ambion) and cleaned up with the Qiagen RNEasy Kit (Qiagen). cDNA was synthesized using Superscript III (Life Technologies). Quantitative PCR (qPCR) was performed with a CFX96 RT-PCR system (BioRad) using primers listed in Supplementary Table S2. Relative fold change was obtained using the ΔΔ*C*q method. Results were normalized to the geometric mean of *RPS13* and *B2M* human housekeeping gene expression.

Gene expression microarray

The Illumina HT-12 V4 beadchip was used for gene expression microarray following manufacturer protocols. Sample intensities were quantile normalized with Lumi software. Using a cutoff of 2-fold change, differentially expressed genes were identified between peroxide-induced senescent cells or replicative senescent cells versus parental nonsenescent CAFs (CAF1-3). Common genes in both comparative datasets were entered into the Gene Ontology PANTHER database to identify genes with secreted products.

Cytokine array and IL8 ELISA

For the cytokine array, conditioned media were derived by incubating 1 million CAF1 cells for 24 hours in serum-free media. The media were used with the Human Cytokine Array, Panel A Kit (R&D systems). For IL8 ELISA, conditioned media were obtained by incubating 50,000 cancer cells or CAF line 5 cells for 24 hours in 0.5% FBS media. Samples were processed with the human IL8 Quantikine ELISA Kit (R&D systems) as per manufacturer's instructions.

***In vivo* experiments**

For orthotopic injections, mice were anesthetized with ketamine (80 mg/kg) prior to flank incision. L3.6pl or Panc1 cells were implanted (500,000 cells) ± CAFs (1 million cells), either orthotopically into the pancreas or subcutaneously into the right flank of 4- to 7-week-old NSG mice. Subcutaneously injected mice had tumor size measurements taken twice weekly and were sacrificed when the largest tumor reached 1.5 cm in greatest dimension. Orthotopically injected mice were sacrificed when the largest abdominal tumors were clearly palpable or at signs of significant illness. Pancreas, lungs, liver, peritoneal nodules, and spleen were submitted for histology. Metastatic foci were identified histologically; foci were considered distinct if they consisted of 5 or more cells and located at least 1 diameter away from another focus.

Results

We derived 5 primary CAF lines to use experimentally, which grow as spindle cells in culture (Fig. 1A). Their myofibroblastic differentiation was confirmed by expression of THY1, α-SMA, PDGFR-β, and vimentin (VIM) on immunofluorescence (Fig. 1B, Supplementary Fig. S2; refs. 2, 3, 23). We confirmed by IHC that THY1 and PDGFR-β localized to the primary PDAC stroma (Supplementary Fig. S3). The cultured CAFs were negative for pankeratin, CD31, and CD45 and thus lacking evidence of epithelial, endothelial, or hematopoietic differentiation (Fig. 1B). CAFs were induced to senesce either by peroxide treatment or by prolonged replication (late passage). Induced CAFs showed cellular enlargement, reduced growth rates, reduced S-phase cells (Fig. 1C and D, Supplementary Fig. S4), higher β-galactosidase activity (Fig. 1E–G, Supplementary Fig. S5), and overexpression of p16 (Fig. 1H), consistent with senescence (13, 14, 24–29).

Effects of senescent CAFs on cancer growth, invasion, and metastasis

To explore the effects of CAFs and senescent CAFs on cancer cell growth, the CAFs were indirectly cocultured in a Transwell format with Panc1 or L3.6pl PDAC cells. Both types of CAFs improved the survival and growth of cancer cells in a low serum environment, as compared with cancer cells cultured alone (Fig. 2A and B). To explore this finding *in vivo*, subcutaneous cancer cell/CAF co-implantation experiments were performed using NSG mice. The addition of either senescent or nonsenescent CAFs resulted in larger tumors for Panc1 and L3.6pl (Fig. 2C and D). Thus, the 2 CAF phenotypes could not be differentiated by their effects on cancer growth.

We next explored the effects of senescent CAF on cancer cell invasion and metastasis. Senescent CAFs demonstrated greater ability to induce Transwell Matrigel invasion of MiaPaca2-YFP and Panc1 cells compared with nonsenescent parental CAFs or blank controls (Fig. 2E and F). Conversely, the nonsenescent CAFs failed to induce significant invasion. When L3.6pl cells were implanted orthotopically into NSG mice pancreas, co-implantation with fibroblasts resulted in similarly sized primary tumors (Table 1). However, co-injected CAFs contributed to additional tumor burden by promoting metastasis. As expected for this cell line, the most common site of metastasis was the liver, representing 51% of all distinct metastatic foci; the rest metastasized to lung (36%) and peritoneum (13%). No splenic metastases were identified. Interestingly, L3.6pl cells co-injected with CAF1-H senescent fibroblasts showed more liver metastases compared with both L3.6pl injected alone and those co-injected with nonsenescent CAF1 fibroblasts (Table 1). When total metastatic foci from all sites were considered, the L3.6pl/CAF1-H co-injected mice had a significantly greater number of metastatic foci than L3.6pl injected alone ($P = 0.01$). Histologically, the metastatic foci were composed of carcinoma cells without human fibroblasts; all associated spindle cells were of mouse origin as confirmed by FISH (Supplementary Fig. S6).

Candidate mediators for the effects of senescent CAFs

The mediators of proinvasive/metastatic effects of senescent CAF towards PDAC are not known, but the senescence-associated secretory phenotype provides a source of candidates. Real-time PCR was performed on a select panel of genes associated with the SASP. *IL8* and *MMP3* were upregulated in the senescent CAFs compared with nonsenescent CAFs. *IL6*, CXC motif chemokine 12 (*CXCL12*), collagen 1A1 (*COL1A1*), and fibronectin (*FN*) were unchanged (Fig. 3A). *CXCL1* trended upward in peroxide-induced senescent CAFs ($P = 0.056$) and was borderline significantly upregulated in replicative senescent CAFs ($P = 0.044$).

CAF1-3 RNAs were analyzed via an Illumina HT12-v4 gene expression microarray. Comparisons of paired nonsenescent/senescent CAFs revealed 279 probes that were differentially expressed (2-fold change difference) between both peroxide- and replication-induced senescent CAFs compared with parental controls (Dataset S1, NCBI GEO accession GSE81368). As the Transwell invasion assay effects were likely mediated by secreted factors, we focused on the subset of differentially expressed genes with secreted products. Gene Ontology PANTHER database

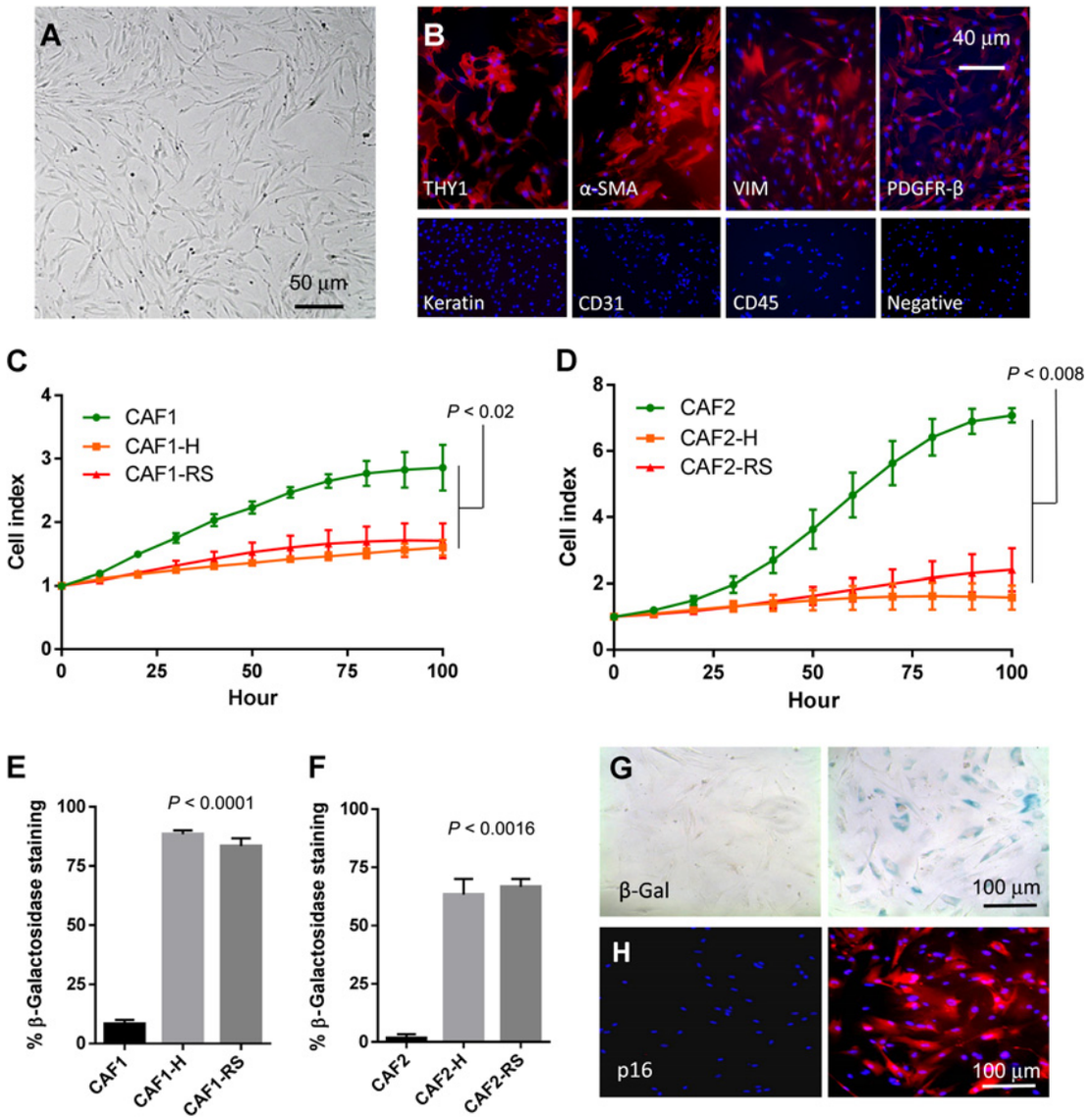

Figure 1.

Primary culture of pancreatic CAFs and the induction of senescence. **A,** Adherent spindle cells grew out in culture over several weeks from primary PDAC samples. **B,** CAF line 1 at passage 5 shows immunofluorescent expression of THY1, α-SMA, VIM, and PDGFR-β, consistent with myofibroblast differentiation. There was no expression of keratin, CD31, and CD45. Cells were visualized by Cy3-conjugated secondary antibody with DAPI nuclear counterstain. **C** and **D,** Induction of senescence by hydrogen peroxide (H) or prolonged replication (RS) reduced growth over 100 hours for CAF line 1 and 2 as measured by the xCelligence cell index system. Comparisons made by linear mixed-effects model of 3 experimental replicates. **E** and **F,** Induction of senescence also increased percentage of the β-galactosidase activity in CAF1 and CAF2 cultures. Comparisons made by ANOVA of 3 experimental replicates in technical triplicates. All error bars represent SE. **G,** Proliferating CAF1 cells (left) and replicative senescent CAF1-RS (right) cells stained by β-galactosidase assay (pH 6.0) showed significant blue positive staining only in the RS cells. This is produced when active lysosomal β-galactosidase cleaves X-gal, a phenomenon seen in senescence. **H,** By immunofluorescence, p16 was absent in parental CAF1 cells (left) and positive in CAF1-RS replicative senescent CAFs (right). Nuclei were counterstained with DAPI.

identified 70 differentially expressed genes which were extracellular or possessed an extracellular region (Dataset S2). Of these, 11 upregulated genes and 7 downregulated genes encoded secreted proteins (Fig. 3B, Dataset S3). The most highly upregulated gene was IL8.

To screen for candidates at a protein level, an ELISA-based cytokine array was performed using CAF conditioned media. This detected higher levels of IL6, IL8, CXCL1, macrophage migration inhibitory factor (MIF), and complement 5 (C5/C5a) in the senescent CAF media compared with nonsenescent CAFs (Fig. 3C). Multiple screening methodologies have identified IL8 to be consistently upregulated by senescent CAFs. We proceeded to perform quantitative ELISA for IL8 using conditioned media of senescent CAFs, nonsenescent CAFs, and cancer cell lines. This showed that senescent CAFs secreted considerably higher levels of IL8 compared with nonsenescent CAFs and cancer cells (Fig. 3D).

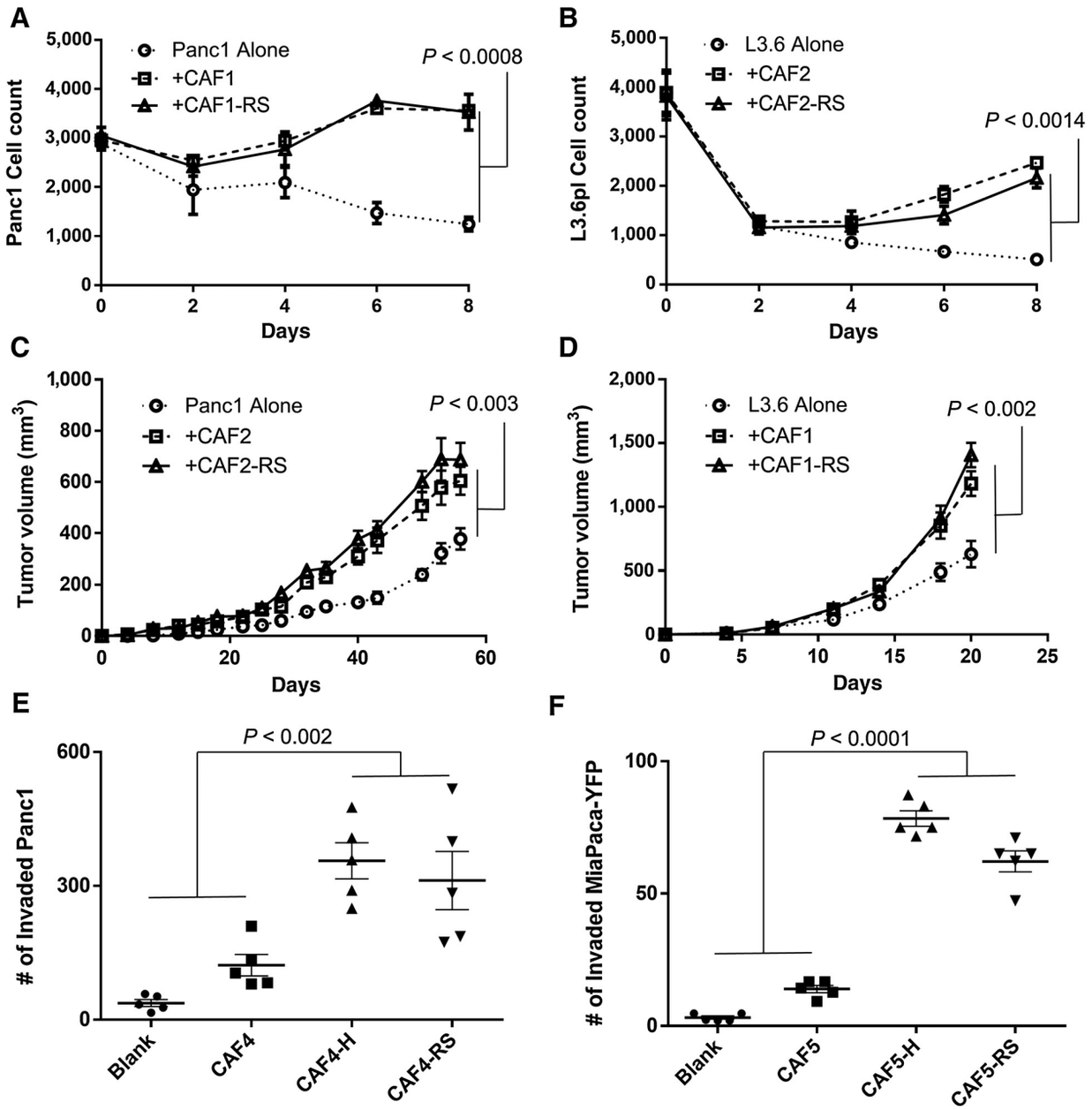

Figure 2.

The effects of CAFs and senescent CAFs on pancreatic cancer growth, invasion, and metastasis. **A,** Indirect coculture with CAF1 or CAF1-RS (20,000 cells in 0.4-μm pore Transwell insert) helped preserve Panc1 cells (5,000 cells in companion plate) under low (0.5%) serum conditions. **B,** Similar results were seen with L3.6pl cells and CAF2 or CAF2-RS. Three experimental replicates with technical triplicates were compared by linear mixed-effects model. Panc1 (**C**) or L3.6pl (**D**; 500,000 cells) injected subcutaneously into the flank of NSG mice grew into larger tumors when co-implanted with CAF or CAF-RS (1 million cells) compared with when injected alone. Statistics by linear mixed-effects model with $n = 6$ mice per group; one mouse excluded in CAF1-RS group due to injection leak. Senescent CAF-H, CAF-RS (60,000 cells/bottom well) induced greater Transwell Matrigel invasion of (**E**) Panc1 or (**F**) MiaPaca2-YFP cells (50,000 cells/insert) than proliferating CAFs or blank negative controls. Statistics by ANOVA with 5 experimental replicates in technical triplicates. All error bars represent SE.

Effects of IL8 on cancer

We proceeded to functionally validate IL8 as a mediator of cancer–CAF interaction. Adding IL8 did not appear to have any effects on the proliferation of MiaPaca2-YFP or Panc1 cells (Supplementary Fig. S7). While we did not possess an immortalized pancreatic CAF line, our group had previously immortalized a lung CAF line (CAF094) with low baseline IL8 secretion (8). By overexpressing IL8 in CAF094 (Fig. 4A), they facilitated greater Transwell invasion of MiaPaca2-YFP (Fig. 4B) and Panc1 cells (Fig. 4C) compared with empty vector controls, supporting a direct role for CAF-derived IL8 in promoting PDAC invasion. The addition of increasing concentrations of SB225002, a

Table 1. Metastatic sites of orthotopically implanted L3.6pl cells

	Arm 1 ($n = 8$)[a] L3.6pl cells alone	Arm 2 ($n = 10$) L3.6pl with CAF1	Arm 3 ($n = 9$) L3.6pl with CAF1H
Pancreas tumor mass (SE)	1.44g (0.42)	1.83g (0.25)	1.42g (0.18)
Mean metastatic foci (SE)			
Liver	0.75 (0.37)	1.3 (0.26)[b]	4.22 (1.04)[b,c]
Lung	0.50 (0.38)	1.6 (0.76)	2.22 (0.78)
Peritoneum	0.50 (0.19)	0.4 (0.16)	0.78 (0.15)
Total	1.75 (0.65)	3.3 (0.8)	7.22 (1.70)[b]

[a]Two mice in the L3.6pl alone arm had peri-pancreatic leaks during injection; 1 mouse in the CAF1H arm died postoperatively. These were excluded from analysis.
[b]Statistical testing by ANOVA with Bonferroni correction: $P < 0.01$ compared with arm 1.
[c]Statistical testing by ANOVA with Bonferroni correction: $P < 0.01$ compared with arm 2.

small-molecule inhibitor of the IL8-binding CXC chemokine receptor 2 (CXCR2), reduced the ability of senescent CAFs to attract cancer cells across a Transwell membrane (Fig. 4D). The inhibitory effect of SB225002 was more pronounced toward senescent fibroblasts as indicated by the lower IC_{50} (Fig. 4E). Proliferation and trypan blue exclusion studies showed that SB225002 exhibited cytotoxicity toward both cancer and CAFs at 2,000 nmol/L but not at lower doses (Supplementary Fig. S8). Reparixin, an inhibitor with strong preference for the IL8 receptor CXC chemokine receptor 1 (CXCR1), mitigated

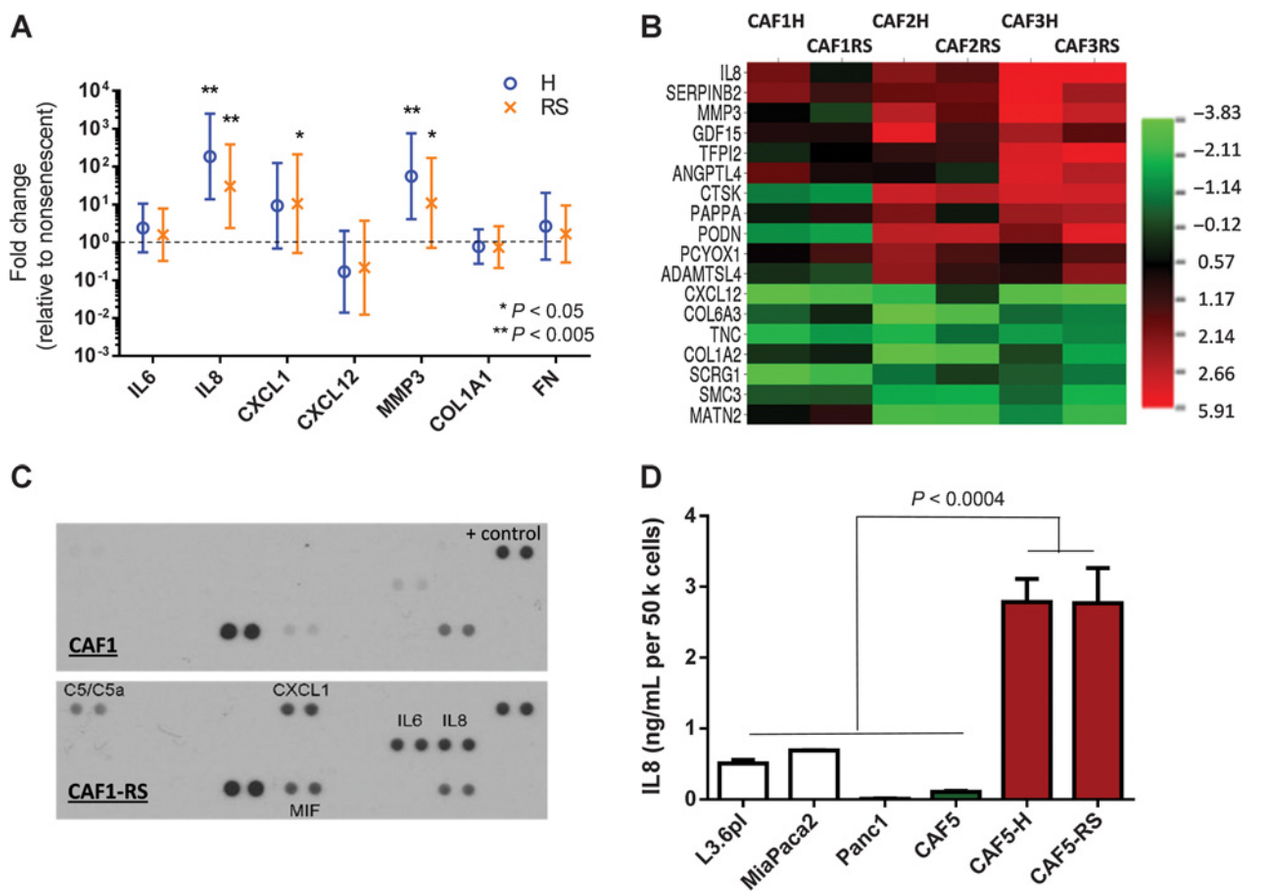

Figure 3.
Screening senescent CAFs for upregulated secreted factors. **A,** qPCR for common senescence-associated secretory phenotype genes showed upregulation of IL8 and MMP3 by senescent CAFs (H or RS) compared with parental lines in 5 biologic replicates (CAFs1-5) done in technical triplicates. Statistics by ANOVA of normalized Cq. Error bars represent 95% CI. Dashed line intersects y-axis at point with no change in expression. **B,** Illumina HT12-V4 microarray with CAF lines 1–3 and corresponding H and RS senescent lines showed that senescent CAFs possessed a number of differentially expressed genes. Differentially expressed genes with secreted products are listed as candidate mediators of senescent CAF–cancer effects. The most highly overexpressed is IL8. Numeric values represent $\log_2$ fold change relative to control CAFs. **C,** Cytokine ELISA array on CAF conditioned media showed increased levels of IL6, IL8, CXCL1, C5/C5a, and MIF in the conditioned media from senescent CAF1-RS compared with CAF1. **D,** IL8 ELISA on conditioned media showed that senescent CAF5-RS and CAF5-H secreted far more IL8 than CAF5 or cancer cells. Statistics by ANOVA, error bars represent SE of 3 separately isolated conditioned media samples.

Transwell invasion to a lesser extent (Supplementary Fig. S9). Reparixin did not exert significant cytotoxicity on MiaPaca2-YFP or CAFs (data not shown).

Stromal senescence in human pancreatic cancer

To explore the clinical relevance of our findings, we examined 98 clinical PDAC cases with available survival data and FFPE tissue. IHC revealed subpopulations of spindle cells in human PDAC stroma to be p16-positive and Ki67 proliferation marker–negative (Supplementary Fig. S10). The entire tumor cohort was then stained by IHC for p16 and IL8. This demonstrated variable proportions of p16 positivity in PDAC stroma (Fig. 5A), as well as variable intensities of IL8 positivity in both carcinoma and stromal cells (Supplementary Fig. S11). Because IL8 is a secreted

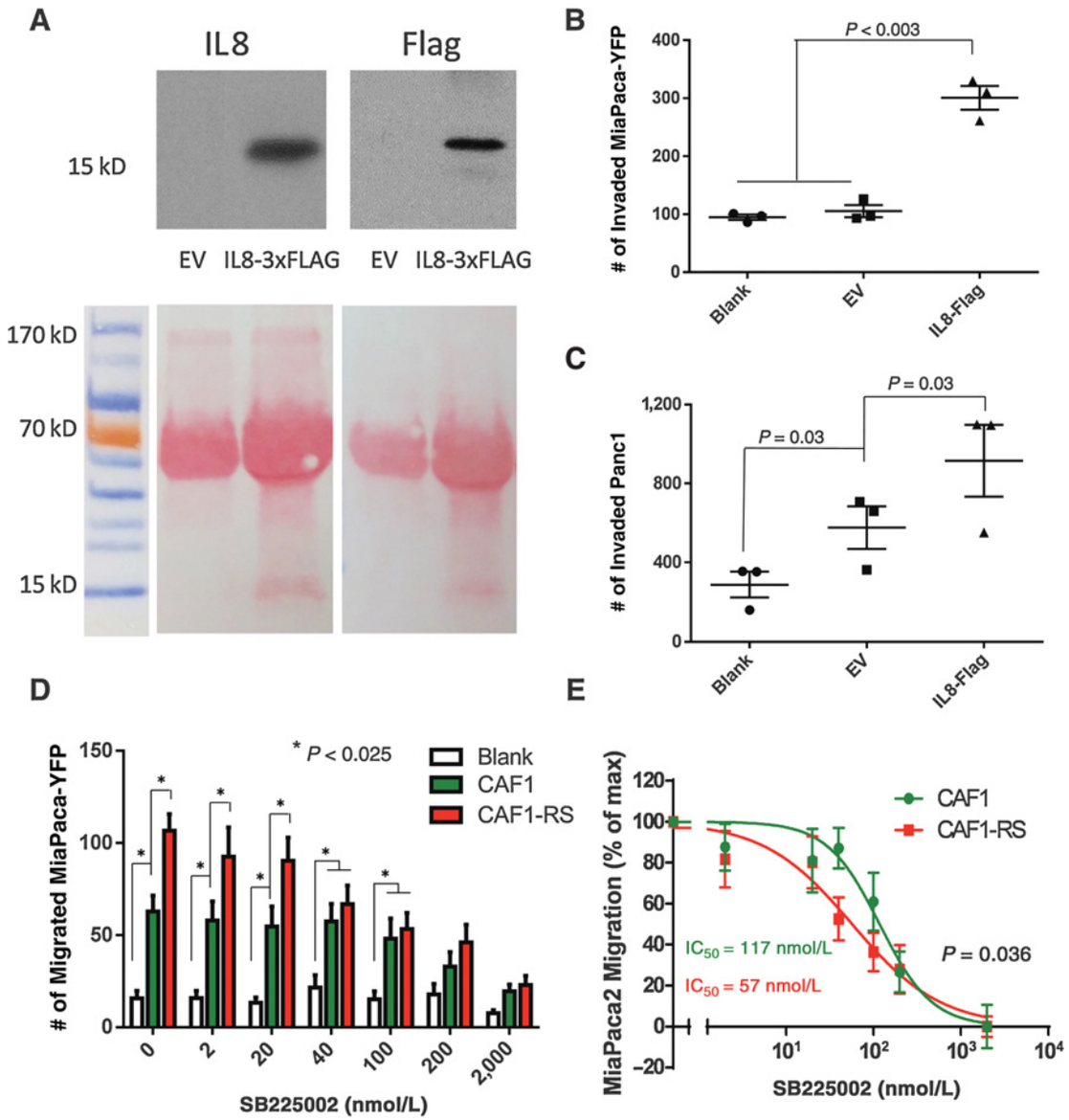

Figure 4.

Effects of IL8 on pancreatic cancer. **A,** IL8 is significantly overexpressed in the conditioned media of CAF094$^{IL8\text{-}3xFlag}$ cells compared with CAF094^{EV} controls by Western blotting. Loading was normalized to total protein assessed by Bradford assay. Bottom, Ponceau S staining of total protein with majority of secreted proteins centered around the 50- to 80-kDa region. 3xFlag-tagged IL8 is detected at about 14 to 15 kDa with IL8 antibody (R&D Systems, MAB208) and anti-FLAG (Cell Signalling, #2368) by Western blotting. **B,** CAF094$^{IL8\text{-}3xFlag}$ (100,000 cells/bottom well) led to greater Transwell Matrigel invasion of MiaPaca2-YFP and Panc1 (**C**; 50,000 cells/insert) compared with empty vector or blank controls. Comparisons made by ANOVA of 3 experimental replicates performed in technical triplicates. **D,** CXCR2 inhibitor SB225002 reduced migration of MiaPaca2-YFP cells (10,000 cells/well) toward CAF1 and CAF1-RS (20,000 cells/well) in a 96-well Transwell migration assay. The difference between senescent CAF1-RS and nonsenescent CAF1 cells was negated after 40 nmol/L or more of inhibitor was added. Five experimental replicates in technical triplicates were compared by 2-way ANOVA. **E,** Normalized inhibition response curve between CAF1- and CAF1-RS–induced MiaPaca2-YFP migration shows that CAF1-RS has a significantly lower IC_{50} for SB225002. Comparison by extra sum-of-squares *F* test. All error bars represent SE.

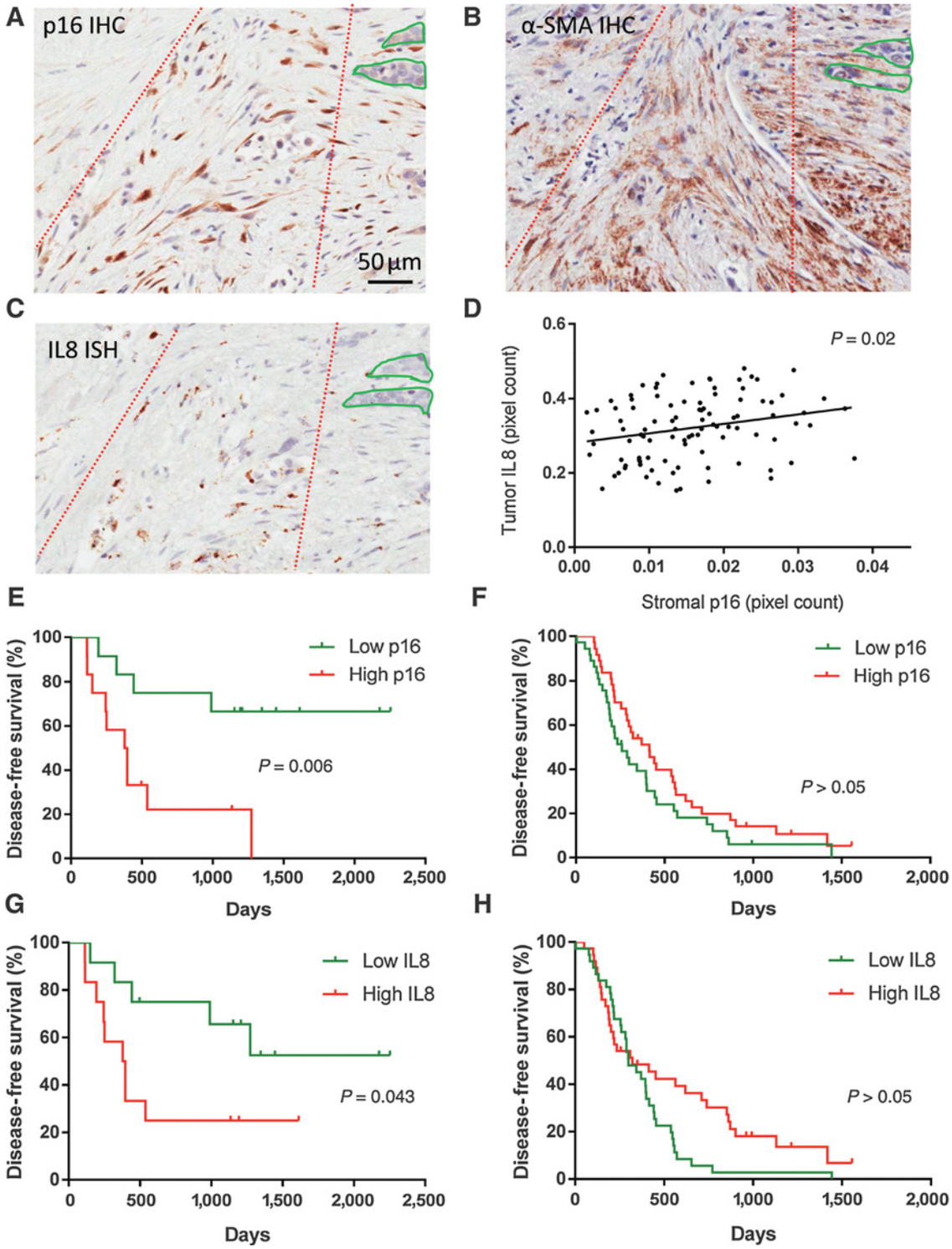

Figure 5.

Stroma senescence is prognostic in human pancreatic cancer. **A,** Stromal p16 in human PDAC by IHC (Ventana, E6H4 clone); carcinoma glands are traced in green outline; densest region of stromal p16 delineated by red dashed lines. **B,** α-SMA (Dako, 1A4) IHC stains the majority of the stromal cells. **C,** RNA ISH shows localization of IL8 RNA (brown signal) in stromal cells in a similar distribution to p16 IHC. **D,** Stromal p16 correlated with tumor IL8 IHC staining in the overall pancreatic cancer patient cohort ($n = 98$) by linear regression. **E,** Stromal p16 correlated with disease-free survival in the stage group 1 cohort (stage IIA or lower, $n = 24$). **F,** Stromal p16 did not correlate with survival in stage group 2 (stage IIB or higher, $n = 74$). **G,** IL8 IHC correlated with disease-free survival in the stage group 1 cohort but not in (**H**) stage group 2. Statistics by log-rank test.

Table 2. Clinical characteristics of patients with pancreatic cancer

	Stage group 1			Stage group 2		
	Low p16 ($n = 12$)	**High p16 ($n = 12$)**	***P***	**Low p16 ($n = 37$)**	**High p16 ($n = 37$)**	***P***
Mean age	63.9	64.5	0.89	64.7	63.8	0.73
Gender			1.00			0.16
Male	5	4		23	16	
Female	7	8		14	21	
Location			0.64			1.00
Head/Neck	10	8		30	31	
Body/Tail	2	4		7	6	
Stage			1.00			1.00
IA	1	1				
IB	3	3				
IIA	8	8				
IIB				36	36	
III				1	1	

NOTE: *P* values obtained by 2-tailed *t* test for age and Fisher exact test in others.

protein, RNA ISH was performed and confirmed that IL8 is primarily expressed by stromal cells. We verified that the stromal cells in PDAC stain intensely with α-SMA, consistent with a myofibroblastic phenotype (Fig. 5B; refs. 2, 6). Furthermore, the IL8 ISH signals appear in a similar stromal distribution to p16 (Fig. 5C).

Because of the relationship between IL8, p16, and cellular senescence, the stromal and tumor IL8 staining were compared with stromal p16 pixel counts. This revealed a positive correlation between stromal p16 and tumor (carcinoma plus stroma) IL8 (Fig. 5D) as well as stromal p16 and stromal IL8 staining ($P = 0.02$). Because of the dismal prognostic implications of lymph node metastasis, we examined the cohort as 2 stage groups. Group 1 ($n = 24$) consisted of patients with stage IIA disease or less (node-negative), whereas group 2 ($n = 74$) consisted of patients with stage IIB disease or higher. Group 1 patients had significantly longer median survival than group 2 (538 vs. 309 days, $P = 0.0009$ by log-rank test). Each group was subdivided into low and high stromal p16 on the basis of median pixel positivity. The clinical characteristics were similar between low and high p16 subgroups (Table 2). For stage group 1, high stromal p16 was associated with markedly reduced disease survival with a univariate Cox regression HR of 4.71 [95% confidence interval (CI), 1.43–14.52; Fig. 5E]. This correlation was not observed in stage group 2 (Fig. 5F). p16 and IL8 showed a trend toward positive correlation in both stage groups ($P = 0.053$ in group 1, $P = 0.086$ in group 2). Importantly, the analysis was conducted with tumor IL8 in relation to disease-free survival in stage group 1 (Fig. 5G). Univariate HR for the high IL8 group compared with low IL8 was 3.13 (95% CI, 1.04–9.40). Again, no statistically significant correlation was found for IL8 in stage group 2 (Fig. 5H).

Discussion

Our results revealed that subpopulations of senescent CAFs exist in both primary cell culture and human PDAC. These senescent CAFs promote PDAC invasion and metastasis, which is mediated, in part, by overexpression of IL8. Higher stromal senescence correlated with reduced survival in patients with early-stage PDAC, indicating that senescent CAFs represent a prognostically relevant fibroblast phenotype in pancreatic cancer.

CAFs form a significant proportion of the PDAC stroma (30, 31). They sustain their myofibroblastic state through autocrine and paracrine signaling, and we confirmed that primary culture CAFs maintained their expression of α-SMA after several passages (5, 32, 33). Tumors with stroma exhibiting higher α-SMA staining or increased extracellular matrix protein production ("activation") have been associated with faster disease progression (6, 34). However, these studies were designed to evaluate intertumoral differences in the stroma and thus are unable to detect intratumoral heterogeneity (6, 34). The assumption has remained that CAFs are relatively homogeneous within any particular tumor and little data exist to challenge this notion. However, the environment in which CAFs exist is not uniform. While proliferating CAFs are responsible for the diffuse desmoplastic PDAC stroma, cancer growth and invasion also cause metabolic perturbation and place oxidative stress on CAFs (35, 36). These conditions are common triggers for cellular senescence, a state which is known to alter fibroblast phenotype (13).

Cellular senescence starts with growth arrest at the G_1–S checkpoint, which is triggered by the p53 or p16/Rb pathways (25, 37, 38). Following this, overexpression of p16 is believed to play a crucial role in establishing the irreversibility of senescence (38–40). While p16 has been used by others as an *in vivo* marker of senescence, we confirmed that p16 can serve as marker of fibroblast senescence both *in vitro* and in human PDAC stroma (41–43). This is supported by the correlation of p16 to other senescence markers such as β-galactosidase and IL8 (13, 14). To our knowledge, we are the first to show the presence of senescent fibroblasts in pancreatic cancer stroma, which confirms that fibroblast senescence is not limited to *in vitro* conditions.

We showed that senescent CAFs increased the invasion and metastasis of cocultured/implanted pancreatic cancer cells. Conversely, nonsenescent CAFs, despite also being activated myofibroblasts, did not demonstrate a significant difference from blank controls. While previous studies have reported that CAFs in general enhance cancer invasion and metastasis, it is not known whether the CAFs used contained a significant proportion of senescent cells (7, 44, 45). Our data clarify that the proinvasive property is predominantly a feature of senescent CAFs, which is consistent with our assertion that senescent CAFs are unique phenotype. It should be noted, however, that nonsenescent CAFs are not inert. In fact, both nonsenescent and senescent CAFs promoted pancreatic cancer growth *in vitro* and *in vivo* compared

with cancer cells growing alone. Nonetheless, senescent CAFs distinguished themselves from other CAFs by influencing not only cancer growth but also invasion and metastasis (15). Local infiltration and distant spread are the most common reasons why PDACs are deemed surgically unresectable, and therefore the effects of senescent CAFs on invasion and metastasis are clinically relevant. On the basis of our coculture experiments, these effects are likely mediated by a secreted product.

Screening by qPCR, gene expression microarray and cytokine ELISA revealed a variety of genes and secreted proteins whose expression are altered in senescent CAFs such as IL8, IL6, CXCL1, C5/C5a, MIF, and MMP3. Of these, IL8 was highly upregulated in senescent CAFs. IL8 is a well-known component of the senescence-associated secretory phenotype (13). It is a proinflammatory chemokine that signals through the CXCR1 and CXCR2 G-protein–coupled receptors to affect many downstream pathways, including PI3K, MAPK, JAK/STAT, and RhoGTPase (46). These pathways regulate proliferation, survival, invasion, cytoskeletal dynamics, and angiogenesis (46). IL8 has been implicated in enhancing PDAC progression through direct effects on cancer cells and through cancer–stromal interaction (47, 48). However, the source of IL8 in pancreatic cancer has not been previously identified. We showed that senescent CAFs secrete considerably more IL8 than cancer cells or nonsenescent CAFs and thus are an important source of IL8 in the microenvironment.

Overexpression of IL8 in a lung fibroblast line induced greater invasion in MiaPaca2-YFP and Panc1, similarly to senescent CAFs. This suggests that IL8 is a proinvasive mediator secreted by senescent CAFs. Inhibition of the CXCR2 IL8 receptor with SB225002 compound mitigated the proinvasive effects of senescent CAFs. The inhibition was more potent for the senescent CAF cocultured cancer cells, as manifested by a lower relative IC_{50}. The higher proportion of IL8 from senescent CAFs likely accounted for this difference. Inhibition of the CXCR1 IL8 receptor with reparixin demonstrated similar but less pronounced trends. Reparixin had the greatest effects at high concentrations where some cross-inhibition of CXCR2 would occur (49). Thus, CXCR2 may play a greater role in mediating the proinvasive IL8 effects in PDAC. These findings not only reveal IL8 to be an important mediator of the cancer-promoting properties of senescent CAFs but also point to the IL8 pathway as a potential therapeutic target.

To address the relevance of stromal senescence in human disease, tissue from 98 cases of primary human PDAC were collected. The correlation between IHC p16 positivity in stromal fibroblasts and IL8 staining suggests that human PDAC stroma contains variable proportions of senescent fibroblasts between patients. The expression of IL8 RNA in stromal cells with high p16 and SMA staining suggests that senescent CAFs are likely a producer of IL8 in PDAC stroma. Therefore, we established that human PDAC exhibits variable degrees of stromal senescence, thus displaying both intra- and intertumoral stromal heterogeneity.

Stromal p16 and IL8 displayed an inverse correlation with disease-free survival in stage group 1 ($\leq$stage IIA) patients. This is consistent with our experimental data showing the proinvasive and prometastatic properties of senescent CAFs, which are risk factors for disease recurrence. While the same relationship was not observed in stage group 2, this is not unexpected. Unlike stage group 1 patients, group 2 patients already have lymph node metastasis. Thus, the influence of stromal senescence on their postresection prognosis is likely outweighed by the dismal outcomes associated with the pre-existing metastatic disease. Overall, our results in early-stage PDAC demonstrate that the cancer-promoting effects of senescent CAFs extend beyond experimental models and possess value as a clinical prognostic marker.

The outcomes for pancreatic cancer are poor and have remained stagnant for decades. Several stromal targeted therapies such as MMP inhibitors, angiogenesis inhibitors, and Hedgehog inhibitors have shown disappointing clinical results, and on occasion, have even accelerated disease (50–53). Recent studies have highlighted the complexity of cancer–CAF interactions. We have characterized senescent CAFs as a distinct phenotype that disproportionately drives PDAC progression, which suggests that cancer stroma is heterogeneous. Pancreatic cancer exerts its morbidity and mortality through aggressive local invasion as well as metastasis, behaviors which are promoted by senescent CAFs through the upregulation of IL8. This raises the possibility of cytokine targeted therapy for pancreatic cancer. We also postulate that these findings may extend to other malignancies as well. Thus, the role of stromal senescence in cancer warrants further study, both to better understand cancer–stromal interaction and to identify novel prognostic markers and therapeutic targets.

Disclosure of Potential Conflicts of Interest

No potential conflicts of interest were disclosed.

Authors' Contributions

Conception and design: T. Wang, R. Navab, M.-S. Tsao
Development of methodology: T. Wang, R. Navab, J. Xu, M.-S. Tsao
Acquisition of data (provided animals, acquired and managed patients, provided facilities, etc.): T. Wang, J. Joseph, J. Xu, A. Borgida, S. Gallinger, M.-S. Tsao
Analysis and interpretation of data (e.g., statistical analysis, biostatistics, computational analysis): T. Wang, F. Notta, C.-Q. Zhu, M.-S. Tsao
Writing, review, and/or revision of the manuscript: T. Wang, F. Notta, R. Navab, J. Joseph, A. Borgida, S. Gallinger, M.-S. Tsao
Administrative, technical, or material support (i.e., reporting or organizing data, constructing databases): T. Wang, E. Ibrahimov, S. Gallinger, M.-S. Tsao
Study supervision: M.-S. Tsao
Other (provided the data on patients): A. Borgida

Acknowledgments

We wish to thank Dr. Dianne Chadwick and the staff of the UHN Tissue Biobank for their assistance in securing pancreatic cancer tissue for this study.

Grant Support

This work is supported by funding from the Cancer Research Society/Pancreatic Cancer Canada/John van Haastrecht Research Grant, the Princess Margaret Center Foundation, the Ontario Institute for Cancer Research/PanCuRx Translational Research Initiative, and the Ontario Ministry of Health and Long Term Care. Tao Wang is supported by the Terry Fox Foundation STIHR Program in Molecular Pathology of Cancer at CIHR (STP 53912). Ming-Sound Tsao is the M. Qasim Choksi Chair in Lung Cancer Translational Research.

The costs of publication of this article were defrayed in part by the payment of page charges. This article must therefore be hereby marked *advertisement* in accordance with 18 U.S.C. Section 1734 solely to indicate this fact.

Received June 6, 2016; revised August 30, 2016; accepted September 14, 2016; published OnlineFirst September 27, 2016.

References

1. The International Agency for Research on Cancer. WHO classification of tumours of the digestive system. 4th revised edition. Lyon, France: WHO Publications; 2010.
2. Sinn M, Denkert C, Striefler JK, Pelzer U, Stieler JM, Bahra M, et al. α-Smooth muscle actin expression and desmoplastic stromal reaction in pancreatic cancer: results from the CONKO-001 study. Br J Cancer 2014;111:1917–23.
3. Yuzawa S, Kano MR, Einama T, Nishihara H. PDGFRβ expression in tumor stroma of pancreatic adenocarcinoma as a reliable prognostic marker. Med Oncol Northwood Lond Engl 2012;29:2824–30.
4. Öhlund D, Elyada E, Tuveson D. Fibroblast heterogeneity in the cancer wound. J Exp Med 2014;211:1503–23.
5. Erez N, Truitt M, Olson P, Hanahan D. Cancer-associated fibroblasts are activated in incipient neoplasia to orchestrate tumor-promoting inflammation in an NF-κB-dependent manner. Cancer Cell 2010;17:135–47.
6. Erkan M, Michalski CW, Rieder S, Reiser-Erkan C, Abiatari I, Kolb A, et al. The activated stroma index is a novel and independent prognostic marker in pancreatic ductal adenocarcinoma. Clin Gastroenterol Hepatol 2008; 6:1155–61.
7. Hwang RF, Moore T, Arumugam T, Ramachandran V, Amos KD, Rivera A, et al. Cancer-associated stromal fibroblasts promote pancreatic tumor progression. Cancer Res 2008;68:918–26.
8. Navab R, Strumpf D, Bandarchi B, Zhu C-Q, Pintilie M, Ramnarine VR, et al. Prognostic gene-expression signature of carcinoma-associated fibroblasts in non-small cell lung cancer. Proc Natl Acad Sci 2011; 108:7160–5.
9. Wang W, Li Q, Yamada T, Matsumoto K, Matsumoto I, Oda M, et al. Crosstalk to stromal fibroblasts induces resistance of lung cancer to epidermal growth factor receptor tyrosine kinase inhibitors. Clin Cancer Res 2009;15:6630–8.
10. Özdemir BC, Pentcheva-Hoang T, Carstens JL, Zheng X, Wu C-C, Simpson TR, et al. Depletion of carcinoma-associated fibroblasts and fibrosis induces immunosuppression and accelerates pancreas cancer with reduced survival. Cancer Cell 2014;25:719–34.
11. Olive KP, Jacobetz MA, Davidson CJ, Gopinathan A, McIntyre D, Honess D, et al. Inhibition of Hedgehog signaling enhances delivery of chemotherapy in a mouse model of pancreatic cancer. Science 2009;324:1457–61.
12. Lee JJ, Perera RM, Wang H, Wu D-C, Liu XS, Han S, et al. Stromal response to Hedgehog signaling restrains pancreatic cancer progression. Proc Natl Acad Sci 2014;111:E3091–100.
13. Coppé J-P, Desprez P-Y, Krtolica A, Campisi J. The senescence-associated secretory phenotype: the dark side of tumor suppression. Annu Rev Pathol 2010;5:99–118.
14. Dimri GP, Lee X, Basile G, Acosta M, Scott G, Roskelley C, et al. A biomarker that identifies senescent human cells in culture and in aging skin *in vivo*. Proc Natl Acad Sci 1995;92:9363–7.
15. Alspach E, Flanagan KC, Luo X, Ruhland MK, Huang H, Pazolli E, et al. p38MAPK plays a crucial role in stromal-mediated tumorigenesis. Cancer Discov 2014;4:716–29.
16. Parrinello S, Coppe J-P, Krtolica A, Campisi J. Stromal-epithelial interactions in aging and cancer: senescent fibroblasts alter epithelial cell differentiation. J Cell Sci 2005;118:485–96.
17. Bavik C, Coleman I, Dean JP, Knudsen B, Plymate S, Nelson PS. The gene expression program of prostate fibroblast senescence modulates neoplastic epithelial cell proliferation through paracrine mechanisms. Cancer Res 2006;66:794–802.
18. Hassona Y, Cirillo N, Heesom K, Parkinson EK, Prime SS. Senescent cancer-associated fibroblasts secrete active MMP-2 that promotes keratinocyte discohesion and invasion. Br J Cancer 2014;111:1230–7.
19. Coppé J-P, Patil CK, Rodier F, Sun Y, Muñoz DP, Goldstein J, et al. Senescence-associated secretory phenotypes reveal cell-nonautonomous functions of oncogenic RAS and the p53 tumor suppressor. PLoS Biol 2008;6:e301.
20. Coppé J-P, Kauser K, Campisi J, Beauséjour CM. Secretion of vascular endothelial growth factor by primary human fibroblasts at senescence. J Biol Chem 2006;281:29568–74.
21. Naldini L, Blömer U, Gallay P, Ory D, Mulligan R, Gage FH, et al. *In vivo* gene delivery and stable transduction of nondividing cells by a lentiviral vector. Science 1996;272:263–7.
22. Zufferey R, Dull T, Mandel RJ, Bukovsky A, Quiroz D, Naldini L, et al. Self-inactivating lentivirus vector for safe and efficient *in vivo* gene delivery. J Virol 1998;72:9873–80.
23. Kisselbach L, Merges M, Bossie A, Boyd A. CD90 Expression on human primary cells and elimination of contaminating fibroblasts from cell cultures. Cytotechnology 2009;59:31–44.
24. Campisi J, d' Adda di Fagagna F. Cellular senescence: when bad things happen to good cells. Nat Rev Mol Cell Biol 2007;8:729–40.
25. Baker DJ, Wijshake T, Tchkonia T, LeBrasseur NK, Childs BG, van de Sluis B, et al. Clearance of p16Ink4a-positive senescent cells delays ageing-associated disorders. Nature 2011;479:232–6.
26. Lawless C, Wang C, Jurk D, Merz A, von Zglinicki T, Passos JF. Quantitative assessment of markers for cell senescence. Exp Gerontol 2010;45:772–8.
27. Mammone T, Gan D, Foyouzi-Youssefi R. Apoptotic cell death increases with senescence in normal human dermal fibroblast cultures. Cell Biol Int 2006;30:903–9.
28. Sherwood SW, Rush D, Ellsworth JL, Schimke RT. Defining cellular senescence in IMR-90 cells: a flow cytometric analysis. Proc Natl Acad Sci U S A 1988;85:9086–90.
29. Mao Z, Ke Z, Gorbunova V, Seluanov A. Replicatively senescent cells are arrested in G1 and G2 phases. Aging 2012;4:431–5.
30. Gore J, Korc M. Pancreatic cancer stroma: friend or foe? Cancer Cell 2014;25:711–2.
31. Luo G, Long J, Zhang B, Liu C, Xu J, Ni Q, et al. Stroma and pancreatic ductal adenocarcinoma: an interaction loop. Biochim Biophys Acta 2012; 1826:170–8.
32. Beilfuss A, Sowa J-P, Sydor S, Beste M, Bechmann LP, Schlattjan M, et al. Vitamin D counteracts fibrogenic TGF-β signalling in human hepatic stellate cells both receptor-dependently and independently. Gut 2015; 64:791–9.
33. Huang L, Xu A-M, Liu S, Liu W, Li T-J. Cancer-associated fibroblasts in digestive tumors. World J Gastroenterol 2014;20:17804–18.
34. Moffitt RA, Marayati R, Flate EL, Volmar KE, Loeza SGH, Hoadley KA, et al. Virtual microdissection identifies distinct tumor- and stroma-specific subtypes of pancreatic ductal adenocarcinoma. Nat Genet 2015;47:1168–78.
35. Martinez-Outschoorn UE, Lin Z, Trimmer C, Flomenberg N, Wang C, Pavlides S, et al. Cancer cells metabolically "fertilize" the tumor microenvironment with hydrogen peroxide, driving the Warburg effect: implications for PET imaging of human tumors. Cell Cycle Georget Tex 2011;10:2504–20.
36. Ohuchida K, Mizumoto K, Murakami M, Qian L-W, Sato N, Nagai E, et al. Radiation to stromal fibroblasts increases invasiveness of pancreatic cancer cells through tumor-stromal interactions. Cancer Res 2004;64:3215–22.
37. Liu Y, Sanoff HK, Cho H, Burd CE, Torrice C, Ibrahim JG, et al. Expression of p16INK4a in peripheral blood T-cells is a biomarker of human aging. Aging Cell 2009;8:439–48.
38. Beauséjour CM, Krtolica A, Galimi F, Narita M, Lowe SW, Yaswen P, et al. Reversal of human cellular senescence: roles of the p53 and p16 pathways. EMBO J 2003;22:4212–22.
39. Kuilman T, Michaloglou C, Mooi WJ, Peeper DS. The essence of senescence. Genes Dev 2010;24:2463–79.
40. te Poele RH, Okorokov AL, Jardine L, Cummings J, Joel SP. DNA damage is able to induce senescence in tumor cells *in vitro* and *in vivo*. Cancer Res 2002;62:1876–83.
41. Collado M, Serrano M. Senescence in tumours: evidence from mice and humans. Nat Rev Cancer 2010;10:51–7.
42. Collado M, Gil J, Efeyan A, Guerra C, Schuhmacher AJ, Barradas M, et al. Tumour biology: senescence in premalignant tumours. Nature 2005; 436:642.
43. Gray-Schopfer VC, Cheong SC, Chong H, Chow J, Moss T, Abdel-Malek ZA, et al. Cellular senescence in naevi and immortalisation in melanoma: a role for p16? Br J Cancer 2006;95:496–505.
44. Olumi AF, Grossfeld GD, Hayward SW, Carroll PR, Tlsty TD, Cunha GR. Carcinoma-associated fibroblasts direct tumor progression of initiated human prostatic epithelium. Cancer Res 1999;59: 5002–11.
45. Orimo A, Tomioka Y, Shimizu Y, Sato M, Oigawa S, Kamata K, et al. Cancer-associated myofibroblasts possess various factors to promote endometrial tumor progression. Clin Cancer Res 2001;7:3097–105.

46. Waugh DJJ, Wilson C. The interleukin-8 pathway in cancer. Clin Cancer Res 2008;14:6735–41.
47. Kuwada Y, Sasaki T, Morinaka K, Kitadai Y, Mukaida N, Chayama K. Potential involvement of IL-8 and its receptors in the invasiveness of pancreatic cancer cells. Int J Oncol 2003;22:765–71.
48. Ijichi H, Chytil A, Gorska AE, Aakre ME, Bierie B, Tada M, et al. Inhibiting Cxcr2 disrupts tumor-stromal interactions and improves survival in a mouse model of pancreatic ductal adenocarcinoma. J Clin Invest 2011;121:4106–17.
49. Allegretti M, Bertini R, Cesta MC, Bizzarri C, Di Bitondo R, Di Cioccio V, et al. 2-Arylpropionic CXC chemokine receptor 1 (CXCR1) ligands as novel noncompetitive CXCL8 inhibitors. J Med Chem 2005;48:4312–31.
50. Provenzano PP, Cuevas C, Chang AE, Goel VK, Von Hoff DD, Hingorani SR. Enzymatic targeting of the stroma ablates physical barriers to treatment of pancreatic ductal adenocarcinoma. Cancer Cell 2012;21:418–29.
51. Jacobetz MA, Chan DS, Neesse A, Bapiro TE, Cook N, Frese KK, et al. Hyaluronan impairs vascular function and drug delivery in a mouse model of pancreatic cancer. Gut 2013;62:112–20.
52. Li X, Ma Q, Xu Q, Duan W, Lei J, Wu E. Targeting the cancer-stroma interaction: a potential approach for pancreatic cancer treatment. Curr Pharm Des 2012;18:2404–15.
53. Evans JD, Stark A, Johnson CD, Daniel F, Carmichael J, Buckels J, et al. A phase II trial of marimastat in advanced pancreatic cancer. Br J Cancer 2001;85:1865–70.